Effect of electrostatic forces on the porosity of saturated mineral powder samples and implications for chalk strength

Meireles, Leonardo Teixeira Pinto; Storebø, Einar Madsen; Fabricius, Ida Lykke

Published in:
Geophysics

Link to article, DOI:
10.1190/geo2018-0724.1

Publication date:
2020

Document Version
Publisher's PDF, also known as Version of record

GEOPHYSICS, VOL. 85, NO. 1 (JANUARY-FEBRUARY 2020); P. MR37–MR50, 10 FIGS., 10 TABLES.
10.1190/GEO2018-0724.1

Effect of electrostatic forces on the porosity of saturated mineral powder samples and implications for chalk strength

Leonardo Teixeira Pinto Meireles[1], Einar Madsen Storebø[1], and Ida Lykke Fabricius[1]

ABSTRACT

Electrostatic forces acting at the particle scale can be an important drive behind water weakening of chalk. Upon the replacement of oil with brine, ions present in the imbibing brine can exchange with ions already adsorbed to the calcite surface, leading to a change in the surface potential. This can cause an increase in the disjoining pressure between particles, either reducing the cohesion of particles connected via contact cement or decreasing friction between free particles. We have assessed the effect of electrostatic forces by measuring pore-water effects on porosity in sediment columns using nuclear magnetic resonance relaxometry. Samples of calcite, quartz, or kaolinite powder were saturated with brines containing ions found in seawater (Na^+, Ca^{2+}, Mg^{2+}, Cl^-, and SO_4^{2-}) at varying ionic strengths and as a nonpolar reference, with ethylene glycol. The difference in porosity between samples saturated with glycol and with brines reflects the disjoining pressure. For calcite samples, saturation with solutions containing divalent cations (Ca^{2+} and Mg^{2+}) lead to higher repulsive forces between the grains, whereas adsorption of SO_4^{2-} counteracts the initially positive surface charge, lowering the repulsive forces. Calcium-based brines induced the highest repulsion, probably due to higher surface coverage of Ca^{2+} than that of Mg^{2+} due to its smaller hydrated radius. For kaolinite, differences in potential between the silica and alumina faces as well as the edges can either lead to repulsion between particles or to flocculation, depending on the ionic strength and ionic species of the fluid. Our results indicate that low-salinity water flooding may lead to kaolinite mobilization within reservoirs. A comparison of the results from our calcite powder experiments with results from mechanical tests performed on chalk samples indicates that electrical double layer-related forces can contribute to the weakening of chalk. Saturating brines for which the repulsion between grains in powder experiments was larger corresponds to weaker chalk samples.

INTRODUCTION

Water flooding, the dominant oil recovery technique since the time of its introduction, has been remarkably successful in the North Sea chalk fields in Norway (Hermansen et al., 2000) and Denmark (Ovens et al., 1998). The recovery mechanisms associated with water injection include reservoir pressure maintenance, viscous displacement, and imbibition. Particularly in highly porous chalk though, injection-water-induced reservoir compaction is a major contributor to the enhanced recovery (Cook and Jewell, 1996; Carles and Lapointe, 2004). Although this so-called water weakening of chalk has been a central theme for petroleum engineers working in the North Sea for at least 30 years, no consensus has been reached with respect to the mechanisms behind it. The compaction has been associated with capillary pressure, chemical dissolution, pressure solution, adsorption pressure, and electrostatic effects.

The capillary pressure mechanism is well understood and has been observed in partially saturated soils: The initially water-bearing chalk is filled by oil in a drainage process, leaving a water film trapped between grain contacts. The surface tension between the water and oil phases creates suction between the grains, which leads to increase in cohesion of the chalk (De Gennaro et al., 2004). Several studies showed that capillary pressure cannot be the main cause behind water weakening: Lord et al. (1998) point out that the

Manuscript received by the Editor 26 October 2018; revised manuscript received 21 July 2019; published ahead of production 07 October 2019; published online 6 December 2019.
[1]Technical University of Denmark, Department of Civil Engineering, DK-2800 Kongens Lyngby, Denmark. E-mail: lepi@byg.dtu.dk (corresponding author); eima@byg.dtu.dk; ilfa@byg.dtu.dk.

residual water in dry chalk is too low to support capillary water menisci. In addition, whereas a water saturation of 5%–10% would be considered to give maximum strength, laboratory tests indicate that weakening can be observed for water saturation as low as 5% (Carles and Lapointe, 2004). By observing water weakening as a function of water saturation even when fully mixed with glycol, Risnes et al. (2005) demonstrated that capillary pressure was not the main mechanism behind water weakening.

Chemical dissolution was discussed by Newman (1983), Gutierrez et al. (2000), Korsnes et al. (2006), Madland et al. (2011), and Nermoen et al. (2015), among others. Most of the observations linking weakening to calcite dissolution or ionic substitution of Ca^{2+} (especially with Mg^{2+}) derive from experiments where chalk cores were subjected to flooding with brines, not in equilibrium with the calcite. Nevertheless, the quasi-instantaneous deformations in chalk experienced during water flooding either through pore collapse or fracture reactivation cannot be explained by this mechanism (Schroeder et al., 1998; Gutierrez et al., 2000; Homand and Shao, 2000; Christensen et al., 2003; Ciantia et al., 2014). Perhaps the strongest evidence suggesting that dissolution is not the main mechanism behind the water weakening of chalk was presented by Katika et al. (2015). In that study, pore collapse stress of chalk saturated with several different brines (sodium chloride, magnesium chloride, calcium chloride, and sodium sulfate) and deionized water was assessed. The weakest samples (exhibiting pore collapse at the lowest stress levels) were the ones saturated with calcium chloride, even though this brine reduces the solubility of calcite due to the common ion effect on its solubility equilibrium.

Pressure solution was suggested by Newman (1983) as a failure mechanism for chalk saturated with equilibrated water (e.g., during depletion of a reservoir). Although pressure solution has been shown to locally promote dissolution of calcite (Hellmann et al., 2002a, 2002b), it causes the contact area between the calcite particles to broaden, so after a brief period in which compaction would be observed, the rock would become stiffer and compaction would be halted rather than furthered.

An adsorption pressure mechanism was proposed by Risnes et al. (2003), who noted that although adsorption to an outcrop chalk occurred for different fluids (water, methanol, glycol, and mineral oil), the strength of the bonding would depend on the water activity of the fluid. According to Risnes et al. (2003), fluid activity correlates with the pressure that the adsorbed phase exerts in the grain contacts "corresponding in many aspects to an increase in pore pressure" that would create a disjoining pressure at the grain contacts. Nevertheless, Cooke et al. (2010) and Bovet et al. (2015) demonstrated that the adsorption pressure for methanol in calcite is higher than that for water, whereas Risnes et al. (2003) found that chalk is weaker when saturated with water than when saturated with methanol.

Electrostatic effects have received much attention in the enhanced oil recovery (EOR) discipline, where it has been used to describe supposed wettability alteration resulting from injection of low salinity and "advanced" brines for which the composition is designed by altering the concentration and ratio of the potential determining ions, or PDIs (Sohal et al., 2016). In addition, within the EOR discipline, low-salinity fluid injection has been deemed to impact electrostatic forces between clay particles, leading to their dispersion or flocculation and possibly enhancing oil recovery (Fogden et al., 2011). It was only recently though, that studies linked water weakening of chalk to a disjoining pressure caused by the electrostatic repulsion between the charged chalk particles (Megawati et al., 2013; Nermoen et al., 2018). Megawati et al. (2013) observe that the weakening of chalk samples saturated with Na_2SO_4 was temperature-dependent, being only observed for samples tested at 130°C. This was credited to a perceived higher adsorption of the sulfate ion on the calcite surface at higher temperatures. Higher adsorption of sulfate would then translate as a higher absolute surface potential and higher disjoining forces between grains. Nermoen et al. (2018) modeled the electrical double layer (EDL)-related forces as electrostatic stress, which was incorporated into the traditional Biot effective stress relation. Studies performed in calcite dispersions (Nyström et al., 2001; Pourchet et al., 2013) indeed indicate a clear correlation between the cohesion of the particle network, the attraction forces forces measured with an atomic force microscope and the zeta potential of the system. It is also relevant to note that, by studying salt crystals growing in confined spaces, Desarnaud et al. (2016) found that the pressure exerted by the crystals onto the confining walls was of electrostatic nature and ion-specific.

The main criticism of the electrostatic forces hypothesis is the suggestion that the magnitude of the repulsion between contacting particles may be too small to impact the cohesive strength of chalk (Risnes et al., 2005; Røyne et al., 2015). Many studies have indeed failed to observe a coherent weakening effect on the cohesive strength of well-cemented reservoir samples (Christensen et al., 2003; Gram and Fabricius, 2015) or for single calcite crystals (Bergsaker et al., 2016). On the other hand, several studies observe water weakening as a reduction of shear strength, yield strength, and dynamic and static elastic moduli for high-porosity (and largely uncemented) chalk and as a reduction in residual strength for indurated chalk (Christensen et al., 2003; Risnes et al., 2005; Megawati et al., 2013; Katika et al., 2015). This suggests that the phenomenon could be linked to a reduction in friction between grains. Though stiffness and strength in chalk are governed by contact cementation, damage in the form of microcracks, open fractures, or pore collapse would allow brine to fill the space between grains and reduce friction through electrostatic repulsion, allowing fractures to slide (in the case of localized fractures) or allowing grains to more easily slide and reorganize (subsequent to pore collapse) (Nermoen et al., 2015). Even though the electrostatic forces are about two orders of magnitude lower than the hydration forces, they are long-range forces. In an experiment in which the calcite surfaces are planar as in the study by Røyne et al. (2015), one can anticipate that hydration forces will be dominant over electrical double layer-related forces but in a natural rock, where the particles are convex, the integration of these two forces over the surface in which they act might result in comparable values.

In this study, we assess the effect of a series of saturating brines on the sedimentation porosity of saturated mineral powders. We expect different porosity in sediment columns saturated with different brines because they will induce different long-range repulsive forces between the solid particles. The minerals are typical in the North Sea chalk: biogenic calcite, quartz, and kaolinite (e.g., Røgen and Fabricius, 2002), and the brines contain mono- and divalent ions commonly found in seawater (sodium, chlorine, sulfate, magnesium, and calcium) at four different ionic strengths. Ethylene glycol-saturated powders were included for reference. Ethylene glycol is a nonionic fluid, so it will not induce electrostatic repulsive forces between solid particles. By measuring the electrical conductivity and

pH of the original brines and comparing to the brines after exposure to the mineral powders, we can assess the chemical processes taking place, such as adsorption/desorption and dissolution/precipitation of mineral phases. The porosity of the sediment column was measured by nuclear magnetic resonance (NMR) relaxometry at two simulated overburden levels, achieved by centrifuging of the samples. Because each of the mineral powders was homogeneous (same density, particle size, and specific surface area) and the density of the various brines and ethylene glycol used were roughly the same (1.0–1.1 g/cm^3), we interpreted changes in porosity between the different solutions and reference samples as a direct observation of repulsive electrostatic forces arising between particle surfaces. These variations are then discussed in terms of changes to the surface potential (affected by ion species, hydrated ionic radius, and concentration) and the length of the EDL (affected by salinity).

This study introduces a novel method that allows the observation of electrostatic repulsive forces in action when a mineral surface is saturated with fluid. The method is simpler and more direct than the current assessment of zeta potential, followed by the modeling of the EDL. To assess whether the observed electrostatic repulsive forces impact the strength of outcrop chalk, we compare our results with published results of mechanical testing of chalk saturated with similar brines.

THE EDL

When a mineral particle is dispersed in water, the electric charges on its surface (caused by broken ionic bonds) will in most cases be unevenly balanced by adsorbing water and ions formed by hydrolysis (Stipp, 1999). As a result, a net charge arises, so that positive and negative sites are found on top of the adsorbed water layer. Electrolytic ions can then adsorb on these charged sites and modify the resulting net charge, forming the inner part of the EDL. The net charge is balanced by counterions so close that the attraction toward the charged surface overcomes the tendency to diffuse away from it due to thermal motion (Van Olphen, 1963; Israelachvili, 2011). This region, where the electrical potential decays exponentially with distance from the surface, constitutes the diffuse part of the EDL.

The interaction between the EDLs of two particles that approach each other, either through Brownian motion or through settling, results in a repulsive pressure between the particles (Figure 1). The resulting pressure can be approximated with the Derjaguin, Landau, Verwey, and Overbeek theory (Derjaguin and Landau, 1941; Verwey and Overbeek, 1948), which considers the short-range Van der Waals forces and the double layer-related forces. The latter are a function of the surface potential (dependent on the number or adsorbed ions and their charge) and the ionic strength of the solution.

Because of their relatively high symmetry and because one crystal form involving the *c*- and *a*-axes would typically prevail, we expect calcite and quartz particles to be similarly charged on all sides. By contrast, kaolinite has low symmetry, so the resulting charges on upper side, lower side, and edges should differ, so that the alumina face tends to be more positive than the silica face, and the edges have negative and positive sites (Gupta and Miller, 2010).

SAMPLE MATERIALS, PREPARATION, AND CENTRIFUGE COMPACTION

Solids

Calcite powder was obtained by crushing a block of chalk from Stevns Kridtbrud. This chalk mudstone sample was collected below the water table and is of Maastrichtian age. It is characterized by having a high carbonate content (99.8%) exclusively in the form of calcite, whereas the noncalcite fraction consists of clay (smectite), quartz, apatite, and mica; feldspar occurs as a trace mineral (Hjuler and Fabricius, 2009). Water-washed kaolin clay and washed, powdered quartzitic sea sand were also used. The chemical composition of solids is displayed in Table 1. The physical characteristics of the solids are displayed in Table 2.

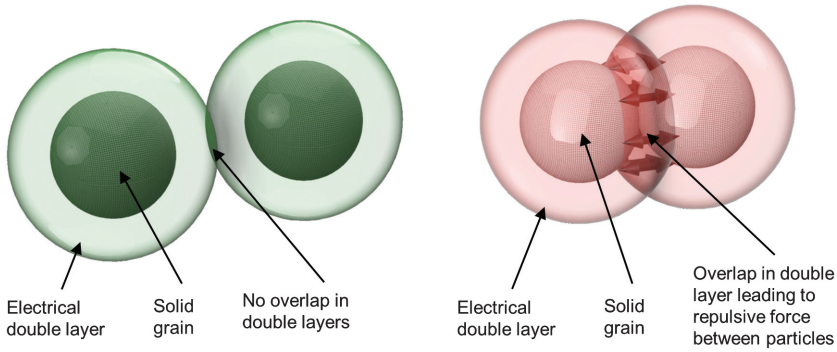

Figure 1. Repulsion between solid particles caused by the interaction between their respective double layers.

Table 1. Chemical analysis of the solids (weight percent).

Component	Sample		
	Calcite[2]	Kaolinite[3]	Quartz[4]
SiO_2 (%)	0.12	45	99
TiO_2 (%)	0.002	0.5–2.5	N.A.
Al_2O_3 (%)	0.028	39	0.3
FeO (%)	0.008	N.A.	N.A.
Fe_2O_3 (%)[5]	—	0.36	0.05
FeS_2 (%)[5]	0.002	—	—
MnO (%)	0.009	N.A.	N.A.
MgO (%)	0.23	N.A.	0.05[6]
CaO (%)	53.6	0.05	0.05[6]
Na_2O (%)	0.023	N.A.	0.1[7]
K_2O (%)	0.03	0.02	0.1[7]

[2]Agate-milled chalk from Stevns Kridtbrud. In addition to CaO, the chalk contains an equivalent amount of CO_2.
[3]KaMin Performance Materials, USA (KaMinHG90). In addition to the listed oxides, kaolinite contains an equivalent amount of H_2O.
[4]Carl Roth, Germany, Art. No. 4651.
[5]In the calcite sample, the measured iron was divided into two fractions (FeS_2 and FeO) based on the presence of pyrite, observed from backscatter SEM/EDS analysis.
[6]CaO + MgO = 0.1%.
[7]$Na_2O + K_2O$ = 0.2%.

Liquids

The brines used to saturate the powders were prepared from reagent-grade NaCl, $CaCl_2$, Na_2SO_4, and $MgCl_2$, as well as water that was deionized and then equilibrated with calcite (24 ppm). Solutions were prepared with four different ionic strengths (Table 3). Ethylene glycol was provided by Fischer Scientific, product number BP230-4.

Table 2. Physical characterization of the solids

Sample	Specific surface area[8] (m^2/g)[9]	Density (g/cm^3)	Grain size (μm)
Calcite	1.89	2.71	1.2[10]
Kaolinite	22.5	2.60	0.4[11]
Quartz	0.92	2.65	1.5–15[12,13]

[8]Derived using Brunauer, Emmet and Teller theory (Brunauer et al., 1938)
[9]The specific surface area was measured by multipoint N_2-BET analysis using a Quantachrome ASiQwin — Automated Gas Sorption Data system. Prior to the measurements, the samples were outgassed in He for 2 h at 60°C.
[10]Equivalent spherical grain radius calculated from BET assuming spherical grains.
[11]Provided by the supplier; measured by the laser diffraction particle sizing technique.
[12]Clausen and Fabricius (2000).
[13]Measured from a scanning electron micrograph image.

Preparation

In total, 102 vials were prepared for the experimental procedure. Samples were assembled by weighing 14 g of the liquids in each vial, adding the solids subsequently (10 g calcite, 14 g quartz, or 8.4 g kaolinite). The flat-bottom borosilicate glass vials had a capacity of 28 ml, a height of 96 mm, and an outer diameter of 23 mm. The vials had a polypropylene screw top and were provided by Fisherbrand. These were non-NMR-specific, and T_2 acquisitions with the empty vial were run to assure that they would not affect the NMR reading. Solids were slowly added to the liquid phase, and the samples were vigorously agitated with a vibrating plate to wet all of the surfaces and avoid the entrapment of air bubbles within the powder. Each sample was then left to rest for a day. For each of the following days, the porosity of the sediment column was measured by NMR relaxometry.

The calcite-bearing samples settled naturally, and we found no significant difference between two subsequent NMR-derived porosity measurements after four days. At this point, the average height of the settlement column was approximately 4 cm, and the differences between samples were due to differences in porosity. This porosity defined the sedimentation porosity. After these measurements were performed, each sample was placed in a centrifuge to simulate a moderate overburden stress σ:

$$\sigma = P_{\text{atm}} + (\rho_{\text{bulk}} - \rho_{\text{fluid}})g_c h, \tag{1}$$

where P_{atm} is the atmospheric pressure, ρ_{bulk} is the bulk density of the sediment column, ρ_{fluid} is the density of the fluids, g_c is the

Table 3. Brine properties at room temperature (approximately 21°C).

Brine salt[14]	Label[15]	Ionic strength[16] (mol/L)	Concentration[16] (ppm)	pH[17]	Conductivity[17] (mS/cm)	Density[18] (g/cm^3)
$CaCl_2$	*UL*	1.83×10^{-3}	6.696×10^{1}	7.99	0.2256	0.9983
	L	1.83×10^{-2}	6.696×10^{2}	7.71	1.859	0.9988
	M	1.83×10^{-1}	6.696×10^{3}	7.37	11.91	1.0045
	H	1.83	6.696×10^{4}	6.47	87.31	1.0578
$MgCl_2$	*UL*	1.83×10^{-3}	5.744×10^{1}	7.91	0.2327	0.9983
	L	1.83×10^{-2}	5.744×10^{2}	7.58	1.876	0.9987
	M	1.83×10^{-1}	5.744×10^{3}	7.41	11.82	1.0032
	H	1.83	5.744×10^{4}	6.78	81.45	1.0460
Na_2SO_4	*UL*	1.83×10^{-3}	8.570×10^{1}	8.04	0.2238	0.9983
	L	1.83×10^{-2}	8.570×10^{2}	7.20	1.814	0.9990
	M	1.83×10^{-1}	8.570×10^{3}	7.31	10.89	1.0064
	H	1.83	8.570×10^{4}	7.27	66.16	1.0748
NaCl	*UL*	1.83×10^{-3}	1.064×10^{2}	8.10	0.05859	0.9983
	L	1.83×10^{-2}	1.064×10^{3}	7.84	0.1787	0.9990
	M	1.83×10^{-1}	1.064×10^{4}	7.72	18.51	1.0060
	H	1.83	1.064×10^{5}	6.98	134.4	1.0693

[14]NaCl: Sigma-Aldrich 31434N-5KG-R; Na_2SO_4: Merck 1.06643; $MgCl_2$: VWR 261237T; $CaCl_2$: Merck 1.02382.
[15]UL indicates an ultralow concentration solution and *L*, *M*, and *H* indicate low, medium, and high concentration solutions, respectively.
[16]Weights of liquids and salts measured in a Sartorius ENTRIS 623i-1x balance with five significant digits.
[17]The conductivity and pH of the brines were measured with a Mettler Toledo SevenCompact Duo pH/conductivity meter, conductivity probe model InLab 731-ISM, and pH probe model InLab expert pro-ISM 30014096.
[18]Calculated with data from Weast (1989): "Concentrative properties of aqueous solutions: Density, refractive index, freezing point depression, and viscosity."

centrifugal acceleration, and h is half the height of the sediment column, so the overburden stress shown in Table 4 is the average stress applied to the sample.

The centrifugal acceleration g_c is calculated as

$$g_c = r\omega^2, \tag{2}$$

where r is the rotational radius and ω is the angular velocity.

For practical purposes, equation 2 can be rewritten in terms of the speed of the centrifuge rotor in revolutions per minute S:

$$g_c = r\left(\frac{2\pi S}{60}\right)^2. \tag{3}$$

After centrifuging, the calcite/brine column had settled to a height of approximately 2.7 cm.

The porosity of the quartz and kaolinite samples did not stabilize one week after the samples were assembled, so we decided to use the centrifuge and compare porosities resulting from two different centrifuging speeds (Table 4). The quartz samples settled to an approximate height of 3.3 cm after the first centrifuging cycle, and kaolinite samples to 2.7 cm. We centrifuged one extra sample of each of these minerals at the indicated speeds for 30 min, measuring the porosity subsequently. After 2 h (from the fifth centrifuging cycle onward), no noticeable difference in porosity was recorded, so all samples were centrifuged for 2 h. The sediment columns settled to a height of approximately 3.0 cm for quartz and 2.3 cm for kaolinite. A flowchart detailing the experimental procedure is shown in Figure 2.

METHODS

Electrical conductivity and pH

Electrical conductivity and pH of the brines were measured prior to the assembly of each sample and immediately after the porosity was measured by NMR. Both probes were calibrated prior to and within a month before the experiments.

NMR and porosity determination

During an NMR acquisition, the transverse relaxation of the signal $M(t)$ can be described by a sum of exponential decays (Dunn et al., 2002):

$$M(t) = M(0)\sum_{j=1}^{\infty} f_j e^{-t/T_{2j}}, \tag{4}$$

where $M(0)$ is the initial amplitude of the transverse magnetic field, T_2 is the transverse relaxation time, t is the time, and f_j represents the fraction of the fluid relaxed at that T_{2j} time.

The initial amplitude of the raw decay curve is directly proportional to the number of polarized hydrogen nuclei in the pore fluid (Dunn et al., 2002); therefore, it is proportional to the volume of fluid itself:

$$M(0) \propto V_{\text{fluid}}. \tag{5}$$

This implies that we can normalize the initial magnetization to the amount of fluid contained in the sample.

The T_2 NMR relaxation is governed by three mechanisms: bulk relaxation, controlled by fluid properties, diffusion in an inhomogeneous magnetic field, and surface relaxation that occurs at the

Table 4. Centrifuge parameters.

	Centrifuge speed (rpm)		Equivalent overburden	
Samples	Acquisition 1	Acquisition 2	Acquisition 1 (kPa)	Acquisition 2 (kPa)
Calcite[19]	0	2000	101	150
Kaolinite[20]	1500	2500	124	166
Quartz[20]	1500	2500	144	201

[19]Calcite samples were centrifuged for 15 min.
[20]Kaolinite and quartz samples were centrifuged for 120 min.

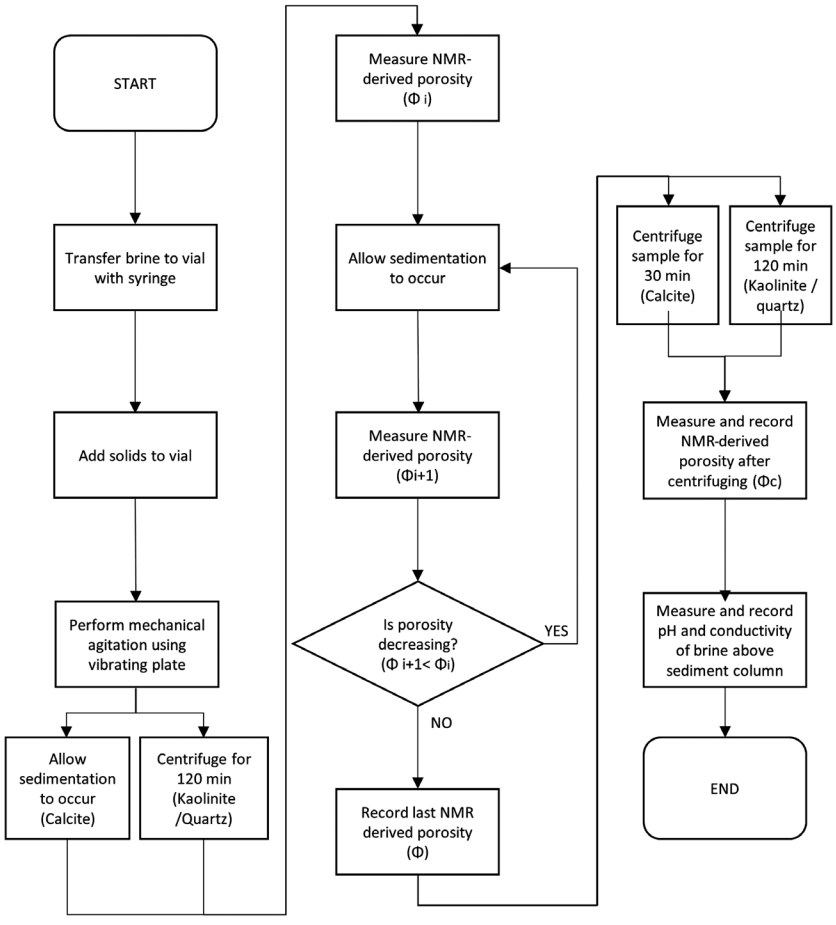

Figure 2. Experiment flowchart.

fluid-solid interface, i.e., when a hydrogen-bearing molecule in the fluid contacts a solid surface (Coates et al., 2000):

$$\frac{1}{T_2} = \frac{1}{T_{2,\text{surface}}} + \frac{1}{T_{2,\text{bulk}}} + \frac{1}{T_{2,\text{diffusion}}}. \quad (6)$$

In our experiment, the contribution of $T_{2,\text{diffusion}}$ to the overall decay is negligible because the field inhomogeneity is minimum in a benchtop probe and solids tested contained no traces of minerals with high magnetic susceptibility, such as magnetite (Keating and Knight, 2007). We also set the interecho spacing (2xTAU) to the lowest achievable value for the probe (110 μs), limiting the distance traveled by the polarized hydrogen nuclei between pulses. We then have

$$\frac{1}{T_2} \approx \frac{1}{T_{2,\text{surface}}} + \frac{1}{T_{2,\text{bulk}}}. \quad (7)$$

All of the hydrogen molecules undergo bulk relaxation, which is not influenced by solid-fluid interfaces. Nevertheless, when surface relaxation is present, the overall relaxation occurs at a faster rate than when only bulk relaxation is present. Even when the solid surface contains a very low concentration of paramagnetic solids (Woessner, 1980), it is possible to differentiate between molecules that underwent surface relaxation on the mineral powder surfaces (the molecules located within the pore space) and the ones that did not because they are present in the free fluid above the powder (Figure 3).

Upon normalizing $M(0)$ to V_{fluid}, the distribution amplitudes represent the amount of fluid relaxed at those particular T_2 times ($V_{\text{fluid}} f_j e^{-t/T_{2j}}$).

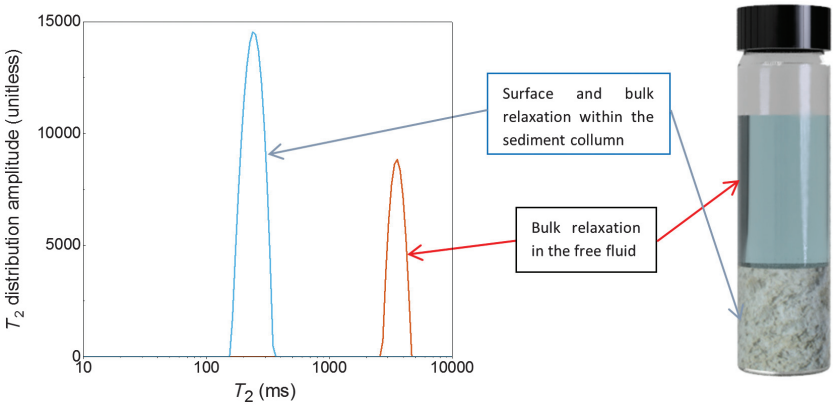

Figure 3. Surface- and bulk-relaxed fluids in the NMR T_2 distribution for a $CaCl_2$ (M) sample.

We can then calculate the volume of the fluid located within the sediment column, which was dominated by surface relaxation V_{sr} by establishing a cut-off T_2 time between the predominantly surface relaxed and the bulk-only relaxed volumes, here equal to 1000 ms:

$$V_{sr} = V_{\text{fluid}} \sum_{j=1}^{j_{\text{cut-off}}} f_j e^{-t/T_{2j}}. \quad (8)$$

The predominantly surface-relaxed volume is equal to the pore volume, i.e., the fluid located within the sediment column:

$$V_{sr} = V_{\text{pore}}. \quad (9)$$

The solid volume of the sample is calculated based on the measured weight of the solid phase m_{solid} and density of the mineral ρ_{min}:

$$V_{\text{solid}} = \frac{m_{\text{solid}}}{\rho_{\text{min}}}. \quad (10)$$

The NMR-derived porosity is then calculated using equation 11, where ϕ_{NMR} is the NMR-derived porosity of the column, V_{pore} is the volume of the pore fraction, and V_{solid} is the volume of the particles:

$$\phi_{\text{NMR}} = \frac{V_{\text{pore}}}{V_{\text{pore}} + V_{\text{solid}}}. \quad (11)$$

During the NMR experiments, all acquisitions were recorded to the same signal-to-noise ratio (S/N) target. Recycle delay was set by running a continuous acquisition and observing how the resulting S/N varied with increments of 5 s. Once the S/N reached a plateau, we inferred that a maximum was reached in the magnetization $M(0)$ of the hydrogen in the samples. The number of echoes was long enough for the bulk fluid in the sample to relax completely. The Carr-Purcell-Meiboom-Gill (Meiboom and Gill, 1958) interecho spacing (2xTAU) value was the lowest achievable by the probe because we anticipated a fast decay of fluid particularly in kaolinite samples due to its high specific surface area (SSA). The gain, $\pi/2$, and π pulses were calibrated immediately prior to the acquisition. The acquisition and processing parameters are shown in Table 5.

Table 5. NMR parameters.

NMR parameters								
Acquisition[21]						Processing[22]		
Recycle delay (ms)	Gain (dB)	S/N	TAU (ms)	Number of echoes	π pulse length (µs)	Weight	Prune points	Pruning mode
30,000	54	>300	0.055	90,909	19.04	0.5	511	Log, averaging

[21]The NMR transverse relaxation decay (T_2) was acquired with a low-field GeoSpec2 NMR Core Analyser using the Carr-Purcell-Meiboom-Gill pulse sequence. The frequency of the GeoSpec2 was centered at 2.25 MHz, and measurements were performed at atmospheric pressure. The temperature of the samples left in the probe stabilized at 30°C.
[22]T_2 relaxation distributions were processed using WinDXP software (Oxford Instruments, UK).

RESULTS

In addition to the porosity measurements that are the focus of this study, measurements of pH and conductivity of the original (unmixed) brines are presented along with the same measurements performed in the brine above the powder after the admixture of the crystal powders and sedimentation. The differences in pH and conductivity are referred to in the "Discussion" section when discussing the processes occurring within the sample, such as adsorption of ions and dissolution.

Electrical conductivity and pH of original brines

The electrical conductivity of all brines increases with ionic strength, although the relationship between ionic strength and conductivity is not linear. There are minor differences in conductivity between the brines with divalent ions, whereas the NaCl brine has a comparatively low conductivity for the two lowest ionic strengths and high conductivity for the two highest ionic strengths (Figure 4).

For the lowest ionic strength, the pH in all of the original brines is close to 7.5 (reflecting the dissolved $CaCO_3$ in the water used to prepare the brines). With increasing ionic strength, the pH of the original brines varies in distinct ways (Figure 5): The pH of $CaCl_2$ and $MgCl_2$ brines diminished with increased salt concentration, whereas the pH of the Na_2SO_4 and NaCl brines remained relatively stable for the whole range.

Electrical conductivity and pH of brines above powder sediment

To assess changes in electrical conductivity in brines exposed to the mineral powders, we plotted the absolute difference in conductivity between the original brine and the brine after exposure to the mineral powders (Figure 6). In calcite samples, the conductivity increases for the two lowest brine ionic strengths, whereas for the two highest ionic strengths, the conductivity of the brines diminishes. Brines exposed to kaolinite powder had a marked increase in conductivity for all brines except for the lowest salinity. For quartz, the conductivity remained relatively stable except for the highest salinity. Here, the $MgCl_2$ and Na_2SO_4 brines showed an increase in conductivity, the $CaCl_2$ brine remained stable, and there was a noticeable decrease in conductivity for the NaCl brine.

Different minerals showed markedly different effects on the pH of the brines. Exposure to calcite had little effect except for brines with high ionic strength, where we found an increased pH for three brines ($MgCl_2$, Na_2SO_4, and NaCl). In contrast, exposure to kaolinite caused some and exposure to quartz caused a marked decrease in pH (Figure 5). According to the manufacturer of the pH probe, an accuracy of up to 0.05 units can be achieved. In our measurements, the repeatability of the pH measurement was within 0.1 pH units except for the high-salinity samples, where repeatability was within 0.2 units. The pH measurements probably did not show an equilibrated system. For instance, the equilibration with kaolinite dissolution may take hundreds of days (Huertas et al., 1999). Nevertheless, these measurements can be used to reflect trends used to identify adsorption on the mineral surfaces.

NMR-derived porosity

The NMR-derived porosity of the samples depends on the mineralogy, overburden state (simulated moderate overburden by centrifuging), ionic strength, and ionic composition of the brines (Figure 7). Generally, ethylene glycol-saturated samples had lower porosity than brine-saturated samples. For simplicity, we refer to the NMR-derived porosity as "porosity" below.

Calcite

The porosity of the brine-saturated calcite powder samples was relatively high for the brines containing Ca^{2+}, and it was relatively low for brines containing SO_4^{2-}; the effect increased with ionic strength. Peak porosity was reached at the ionic strength of 1.83×10^{-2} mol/L for all of the samples with the exception of the $CaCl_2$, for which the peak porosity was reached at 1.83×10^{-1} mol/L. For the samples representing a moderate overburden state (150 kPa), the pattern was roughly shifted to lower porosity.

Kaolinite

The porosity generally increased with the increasing ionic strength, but the pattern is not uniform. For a given ionic strength, samples containing divalent cations had relatively high porosity and samples with a divalent anion had relatively low porosity. The effect increased with ionic strength up to 1.83×10^{-1} mol/L and then decreased again. For the samples with the most dilute brine (*UL*), little difference in porosity was seen between the two levels of overburden (124 and 166 kPa).

Quartz

For all brines, the porosity decreased from the lowest to second lowest ionic strength (1.83×10^{-2} mol/L) and then it increased with the increasing ionic strength. The samples saturated with sodium chloride brine tended to have relatively high porosity, whereas the samples saturated with sodium sulfate brines tended to have relatively low porosity. For the samples representing a moderate overburden state (201 kPa), the pattern was shifted to lower porosity.

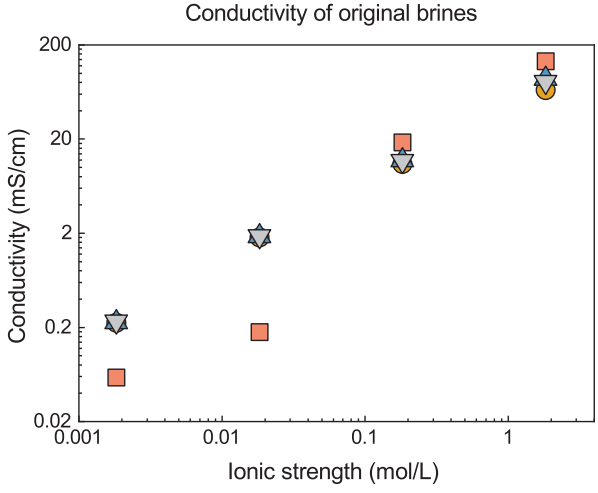

Figure 4. Conductivity of brines prior to sample assembly: $CaCl_2$ (△), $MgCl_2$ (▽), Na_2SO_4 (○), and NaCl (□).

ANALYSIS OF RESULTS

Electrical conductivity and pH of original brines

Out of the four salts used for preparing the brines $CaCl_2$ and $MgCl_2$ are derived from weak bases and a strong acid, Ca^{2+} and Mg^{2+} will thus form aqueous complexes with the hydroxide ion formed by auto-ionization of the water, whereas Cl^- will remain free, leading to a surplus of H_3O^+. With the increasing ionic strength, the pH will decrease, and for the highest ionic strength, it will become acid. The salt Na_2SO_4, on the other hand, is derived from a strong base and a weak acid, so Na^+ will remain free, while SO_4^{2-} will form an aqueous complex with H_3O^+, resulting in an excess of OH^- ions in solution. This trend toward the more basic was probably counteracted by dissolution of CO_2 present in the atmosphere into the brine because we find that the pH of the Na_2SO_4 solution is stable for all values of ionic strength. The salt NaCl is derived from a strong base and a strong acid, and we anticipate no interaction with the water. We find that the pH of the NaCl brine is relatively stable throughout the range with the exception of the high-salinity brine, for which a decrease to a near-neutral pH was found. This indicates that the Ca^{2+}, OH^-, and HCO_3^- formed by the dissolution of calcite no longer control the pH, probably due to their decreased activity in the strong solution.

Porosity of settlement columns and electrical conductivity and pH of brines above the powder sediment

Calcite

Among the three solid phases included in this study, calcite is the most soluble mineral and is also the most relevant for chalk. To validate our assumption that the porosity changes in the sediment column are largely dictated by the electrostatic forces and not by the dissolution of calcite/precipitation of other minerals, chemical reactions occurring in the sample must be assessed, and indeed we find a decrease in electrical conductivity for the strongest brines (Figure 6). This suggests a net precipitation of salts in these samples. An alternative explanation involving adsorption of divalent ions is less likely because porosity data suggest full coverage of the surface sites already at lower ionic strength. The increase in conductivity for three of the brines with the lower ionic strength probably also reflects the dissolution of calcite.

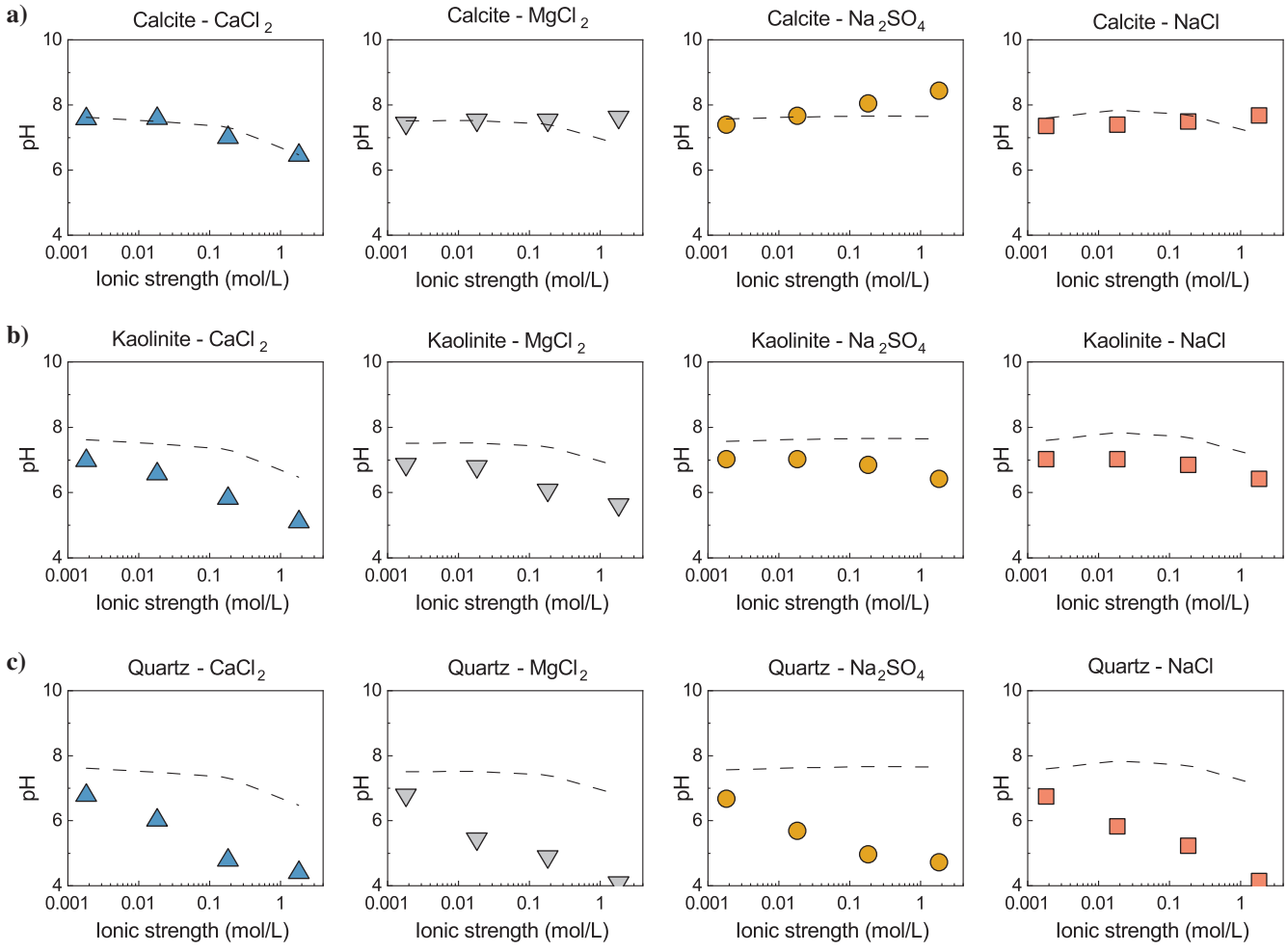

Figure 5. The pH of the original brine (line) and the pH of brines exposed to calcite (a), kaolinite (b), and quartz (c) powder measured after the tests (symbol) versus their ionic strength.

$CaCl_2$ *brines*

There is little difference between the pH of the original brine and after mixing with the calcite powder (Figure 5). This is largely due to the common ion effect. The Ca^{2+} ion brought by the calcium chloride solution prevents dissolution of the calcite, making these samples particularly suitable for investigating the effects of the electrostatic forces on the settling behavior of the sediment column. The divalent Ca^{2+} ion adsorbs to the calcite surface and generates the largest repulsive forces, resulting in the high porosity observed for this series (Figure 7), and the porosity reaches its maximum value when the calcite surface is saturated with Ca^{2+}. Our data indicate that this occurs at an ionic strength in the interval $1.8 \times 10^{-2} - 1.8 \times 10^{-1}$ mol/L (Figure 7), corresponding to a Ca^{2+} concentration of 0.006–0.06 M in agreement with the value of 0.035 M obtained by Song et al. (2017) through zeta potential measurements of calcite in similar brines. An increase in concentration beyond this point will not significantly change the charge on the mineral surface, but it will cause a contraction of the EDL, reducing the range in which the repulsive forces act, thus leading to a decrease in porosity as we indeed find for the sample with the highest concentration when measured after sedimentation (Figure 7). After centrifuging though, the medium (*M*) and high (*H*) concentration samples display very similar values of porosity, indicating that the shorter range Coulomb forces eclipse the effect of the length of the EDL.

$MgCl_2$ *brines*

Even though the Mg^{2+} ion shares the same charge as the Ca^{2+} ion, it is not adsorbed to the same extent due to its larger hydrated size (Tansel et al., 2006). This reflects in a lower zeta potential measured for the same concentrations (Song et al., 2017) and the lower porosity when compared with the $CaCl_2$ series in this study (Figure 7). We observe an increase in pH of the strongest magnesium chloride brine after exposure to calcite. This may be caused by precipitation of the unstable but kinetically favored $MgCO_3$, which will cause a release of OH^- from the hydrated Mg-ion.

Na_2SO_4 *brines*

The sodium sulfate experiments gave the lowest values of porosity in the range of ionic strengths studied. Zeta potential measurements performed over a range of concentrations for this brine (Song et al., 2017) suggest that the SO_4^{2-} ion adsorbs onto the calcite surface, driving the zeta potential down. At the final overburden state and the highest ionic concentration, there is virtually no difference between the porosity measured on the ethylene glycol sample (for which electrostatic forces are negligible) and the sodium sulfate sample, indicating that the sample is close to its point of zero charge (PZC). At high concentrations, the pH of the sodium sulfate brines after mixing with calcite differs significantly from pH of the original brines, approaching the equilibrium pH of the water-calcite system with pCO_2 fixed at $10^{-3.5}$ atm described by Madsen (2001). Apparently, the presence of calcite prevents CO_2 from the atmosphere from totally counteracting the basic effect of the sulfate ion.

NaCl brines

The porosity of the sodium chloride-saturated samples is close to the magnesium chloride series, in agreement with zeta potential measurements performed by Song et al. (2017). Even though sodium is generally considered an indifferent ion (Pierre et al., 1990; Madsen, 2001), meaning that it would not adsorb onto the calcite surface, Ca^{2+} ions will be adsorbed to the calcite (because the brines were prepared with $CaCO_3$ equilibrated water), explaining the repulsive potential of the series. One can observe that the increase in ionic strength results in a decrease in the range of repulsive forces caused by the contraction of the EDL. In the original brine, the high salt concentration caused the activity of Ca^{2+}, HCO_3^-, and OH^- to go down. This effect is counteracted by the presence of calcite and indicates that some calcite must have gone into dissolution.

Kaolinite

To interpret changes in porosity and pH of the kaolinite samples, one has to consider the distribution of charges on the basal surfaces and the edge of the crystal. The reduction in pH of all brines after exposure to kaolinite reflects that neutral water molecules and cations present in the brine (Ca^{2+}, Mg^{2+}, Na^+) substitute H_3O^+, on the mineral edge and the basal surfaces (Ma and Eggleton, 1999) (Figure 5). It is noticeable that the shift in pH is more pronounced for brines containing divalent cations, reflecting that either each divalent cation causes more release of hydronium ions than the monovalent ions per adsorbed site and/or that they achieve better site coverage. Ferris and Jepson (1975) reported higher adsorption of

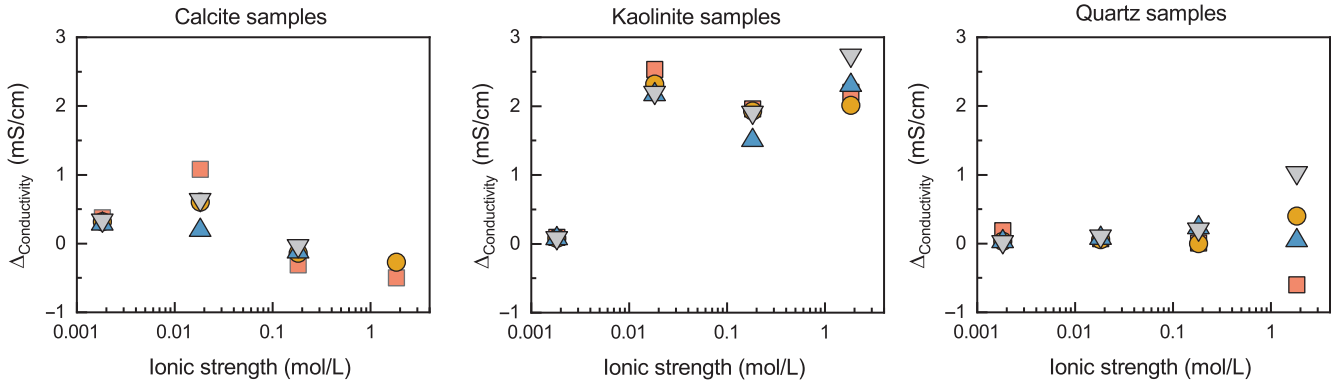

Figure 6. Changes in conductivity of the brines (prior to sample assembly — after mixing with mineral powders): $CaCl_2$ (△), $MgCl_2$ (▽), Na_2SO_4 (○), and NaCl (□).

calcium ions on kaolinite when compared to sodium ions. Yukselen and Kaya (2003) fond that the zeta potential (which reflects the overall charge of the kaolinite) of samples exposed to brines with monovalent ions (NaCl and LiCl) is more negative than for samples saturated with divalent ions ($CaCl_2$ and $MgCl_2$). The pattern of pH and conductivity indicates that more than one hydronium ion is displaced when a monovalent ion is adsorbed, probably due to the fact that the hydrated radius of sodium is larger than the H_3O^+. Because more hydronium ions are released than metallic cations are adsorbed, there is a marked increase in the ionic strength of the solution, which translates into an increase in conductivity for the samples where this exchange occurs (in the *UL* sample, there were too few cations to replace the H_3O^+). Another contribution to the conductivity increase might come from the dissolution of kaolinite (Huertas et al., 1999).

At the lowest ionic strength (*UL*, 1.83×10^{-3} mol/L), it is noticeable that the porosity is higher than that of ethylene-saturated samples and that there is virtually no difference in porosity between the two levels of simulated overburden (Figure 7), indicating that the electrostatic repulsive forces control the settling porosity and that the charges on all surfaces are negative, in agreement with zeta potential measurements performed by Gupta and Miller (2010) and Liu et al. (2013). As the ionic strength is increased, the porosity behavior is strongly influenced by the cation type: On the low (*L*), medium (*M*), and high (*H*) ionic concentrations, the sediment column subjected to brines containing divalent ions (Ca^{2+} and Mg^{2+}) have an increase in porosity, denoting that the charge in the alumina face of the kaolinite has shifted from negative to positive for these samples (Gupta and Miller, 2010; Figure 7a). The shift is also reflected in a reduction of pH of the brines (Figure 5). This can lead to the formation of a flocculated "stair-stepped cardhouse" (O'Brien, 1971), when the positively charged alumina face of a kaolinite particle attaches to the edge of a second, which is expected to have a negative potential throughout the pH range observed in our tests (Liu et al., 2013). It is also observed that the higher the difference in potential is between the positively charged alumina face and the negatively charged edge, the greater the porosity because the flocculation of the kaolinite will occur at a faster rate, settling as a more "voluminous" sediment as classically described by Van Olphen (1963).

The polarity change of the alumina face occurs at a higher concentration for the samples saturated with monovalent brines: The drop in porosity seen between the *UL* and *L* samples suggests that the absolute value of the surface potential falls but is still in the negative field, leading to a smaller repulsive force between grains. For the subsequent ionic strengths, the porosity increases, denoting that the shift in surface charge polarity has occurred and the stair-stepped cardhouse fabric is formed. The effect of the change in charge polarity is further corroborated by a simple visual examination of the samples: For the two least-concentrated Na_2SO_4 saturated samples, the top of the sediment column appears cloudy, reflecting the repulsive behavior of the particles (Figure 8a), whereas, in the *M* and *H* samples, there is a clear distinction between the solid sediment and fluid phase. In addition, in the latter samples, the grains resist movement when the vial is shaken moderately, whereas, in the *UL* and *L* samples, they promptly go into suspension. For $CaCl_2$, the cloudiness is only noted for the *UL* samples, whereas in all others, there is a clear distinction between

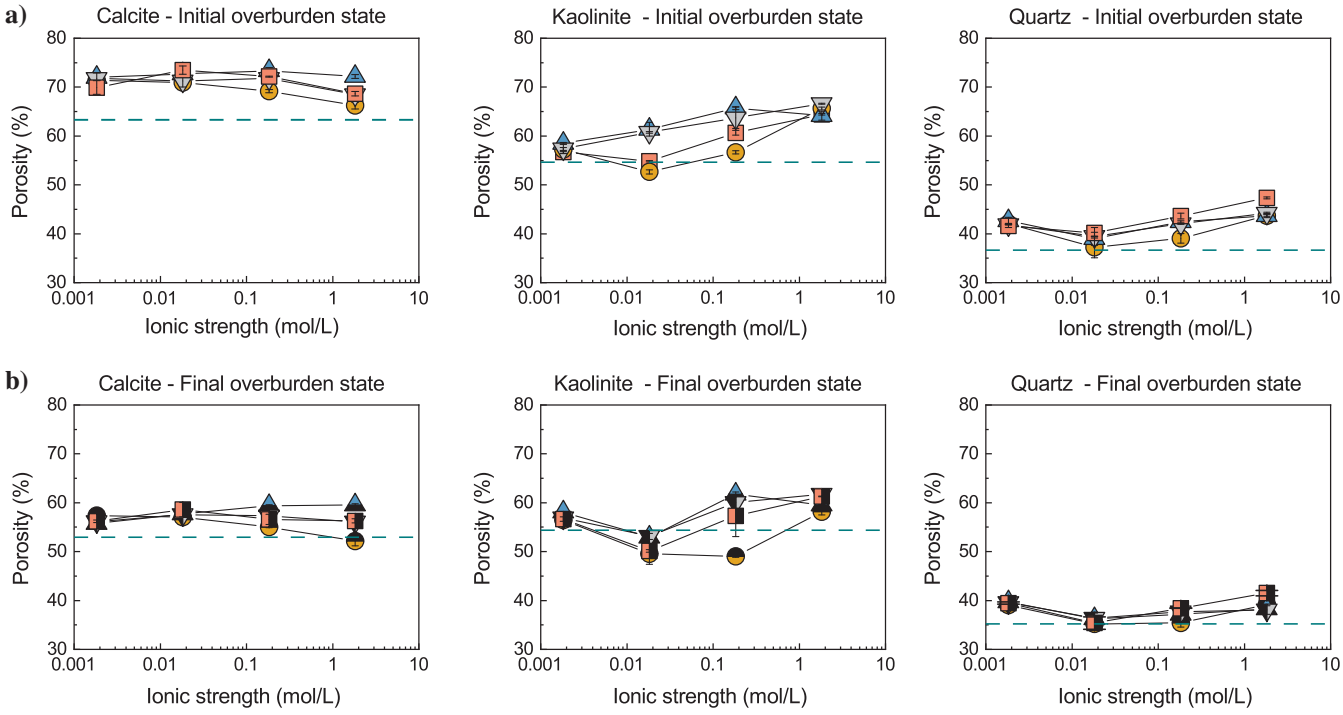

Figure 7. Critical porosity of mineral powder column at the initial state ([a] calcite samples overburden ≈ 101 kPa*, kaolinite ≈ 124 kPa*, and quartz ≈ 144 kPa*) and the final state ([b] calcite samples overburden ≈ 150 kPa *, kaolinite ≈ 166 kPa*, and quartz ≈ 201 kPa*). Brines are $CaCl_2$ (△), $MgCl_2$ (▽), Na_2SO_4 (○), and NaCl (□). The symbols indicate the mean of two measurements (in two distinct samples). The reference line (red, dashed) represents the average between two porosity measurements of samples saturated with ethylene glycol. *Reference pressure ≈ 0.1 MPa.

phases (Figure 8b). Porosity of the *L* samples for Ca^{2+}- and Mg^{2+}-bearing brines show distinct trends between the initial and final overburden states. It is likely that the increased stress applied during the final loading of the *L* samples was enough to collapse the stair-stepped cardhouse fabric because the attraction forces in these samples would be comparatively weaker due to the low positive charge of the alumina face.

Contrasting with the behavior of the other brines, $CaCl_2$ causes a drop in porosity for the high-ionic-strength sample. This suggests that full coverage of the surface sites was already achieved at medium ionic strength and increasing the ionic concentration caused the EDL to contract. Differently from what is observed for the calcite and quartz samples, the porosity of the ethylene glycol samples is not the lowest recorded in the series, indicating that repulsion between the particles occurs even in the absence of adsorption of charged ions from an electrolyte solution, reflecting the uniform charge on the basal plans, which cannot be balanced by distorted molecules of adsorbed water as is the case for quartz and calcite.

Quartz

When exposed to water, an EDL arises around quartz particles due to positive and negative sites reacting with water and generating a net charge. In that situation, the zeta potential assumes increasingly negative values with increasing pH. Ion-specific effects are also present (Yukselen and Kaya, 2003), which may lead to reversal of the quartz surface charge upon increase in concentration (Quan et al., 2012; Lu et al., 2017). We find that ion exchange primarily occurs with the cations, resulting in the release of H_3O^+ as reflected in a decrease in pH with the increasing ionic strength (Figure 5). Even though the electrical mobility of the hydronium ion is much larger than that of the other cations in solution (about five times), the simple 1:1 replacement of a hydronium with a metalic ion at the mineral surface is not enough to cause drastic changes in conductivity. For instance, at pH = 4 (measured for the high-salinity brines), the concentration of hydronium in solution is approximately 10^{-4} M (considering an activity coefficient equal to 1), whereas the ionic strength of the solution is 1.83 M.

At high pH and low cationic concentration, the quartz surface is net negative, and the resulting porosity is higher than that of the neutral ethylene glycol (Figure 7). As the ionic strength increases and pH decreases, the point of zero charge (PZC) is reached (near the ionic strength of 1.83×10^{-2} mol/L), and the porosity is similar to that of ethylene-saturated sediments. With the further increase in ionic strength, quartz particles become positive and the resulting porosity increases (Figure 7).

Correlation between EDL-related forces assessed in this study and mechanical weakening of chalk

Few studies have compared the strength and stiffness of chalk saturated with simple brine solutions (containing only one dissolved salt). The focus is usually placed on modified seawater injection because this is where the industrial application (reservoir flooding) lies. This section will focus mainly on the results obtained by Risnes et al. (2003, 2005), Megawati et al. (2013), and Katika et al. (2015).

Analysis of the data presented by Risnes et al. (2003) (Figure 9) is hindered by the lack of overlapping data points acquired with different brine compositions (the data were presented as yield strength, as a function of water activity). Nevertheless, a separate analysis of the $CaCl_2$ and NaCl series (linear approximation) reveals that the water weakening effect on the chalk saturated with calcium chloride is more significant than that on the chalk saturated with sodium chloride of similar water activity. This behavior suggests that the weakening is indeed ion-specific.

Katika et al. (2015) assessed the strength of outcrop Stevns chalk by measuring the yield strength of core samples saturated with the ionic species (although a single molar concentration was used), which is also used in this study (Figure 10b). Their results contradict the hypothesis that the activity of water control chalk strength because samples saturated with deionized water (Activity = 1) were the strongest among the tested samples. The ionic strength of the brines used in the remaining tests was of 1.83 mol/L; the same ionic strength used on the samples labeled high concentration (*H*) in this study. Comparing the results from the two studies, we find an inverse correlation between the disjoining pressure (measured as changes in porosity) assessed in the chalk powders and the strength

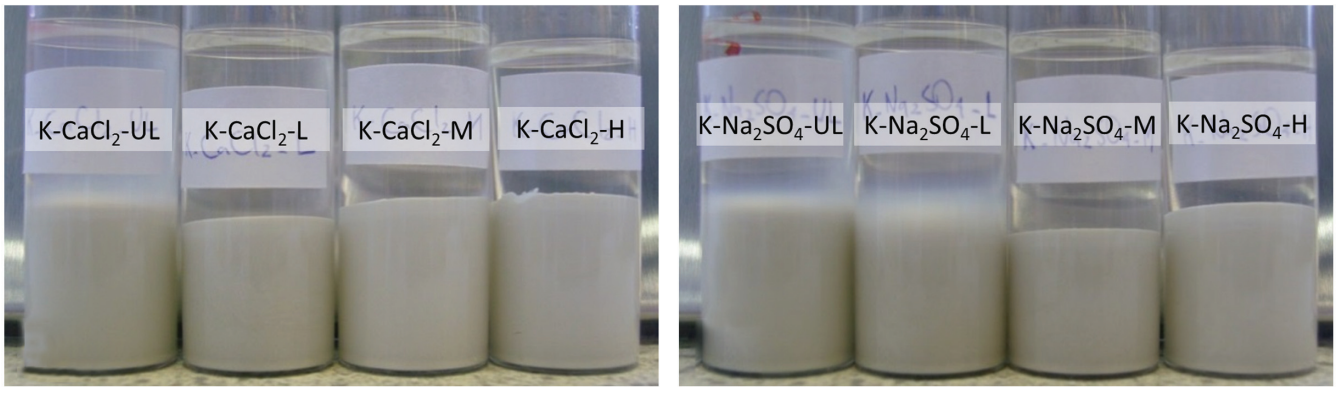

Figure 8. Evidence of charge reversal in the alumina face of the kaolinite at different brine concentrations. (a) In the $CaCl_2$ series, all surface charges (edge, alumina face, and silica face) are negative in the *UL* sample. (b) In the Na_2SO_4 series, this behavior is observed in the *UL* and *L* samples. When all of the surfaces are negative, we see a cloudy appearance of the top of the solid column: The electrostatic repulsive forces between particles with the same polarity drive the particles into suspension. When the charge of the alumina face becomes positive, a stair-stepped cardhouse fabric is formed and the sediment exhibits cohesion. Samples shown in the pictures are in their final overburden state.

of the chalk cores from yield measurements, except for the samples saturated with Na_2SO_4.

It is clear that the weakening observed on Na_2SO_4 saturated samples tested at room temperature by Katika et al. (2015) (Figure 10b) is not mached by the action of electrostatic repulsive forces shown in Figure 10c. Megawati et al. (2013) did not observe weakening in Liège chalk samples saturated with Na_2SO_4 brine, when mechanically tested at room temperature. In their study, the weakening observed in Na_2SO_4-saturated samples only occurred at increased temperatures. Sulfate induced weakening observed by Katika et al. (2015) is almost certainly due to the comparatively higher concentration of sodium sulfate, which induces higher adsorption of the sulfate ion on the calcite surface (Al Mahrouqi et al., 2017). The weakening therefore can still be explained in terms of EDL-related disjoining forces. The lack of correlation between the disjoining pressure measured in this study and the weakening observed by Katika et al. (2015) is likely due to differences in pH between the two different experiments: in a geomechanical test, such as performed by Katika et al. (2015), the samples are placed in a closed Hoek cell, not exposed to atmospheric air. In such a system, one could expect a pH of 10 and relatively low Ca^{2+} concentration (Madsen, 2001). We measured a pH of 7.5–8.5 in our calcite samples saturated with sodium sulfate, indicating that the system is open. For this relatively low pH one could expect a higher Ca^{2+} concentration in the brine, which would adsorb and thus counteract the reduction of the surface potential brought by the sulfate ion.

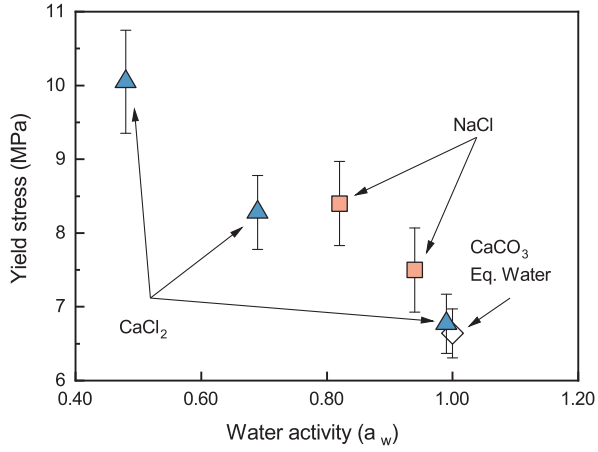

Figure 9. Peak strength of Liège chalk samples saturated with $CaCl_2$, NaCl, and calcite-equilibrated water. Samples were loaded at quasi-hydrostatic conditions, with $K = 0.9$ (adapted from Risnes et al., 2003).

DISCUSSION

The results presented in this study, namely, the impact of saturating fluid on settling porosity, flocculation behavior, and chalk strength of soft chalk, have implications in the understanding of the mechanical strength of consolidated chalk. These results can be used to predict mobilization of clays in oil reservoirs and anticipate geomechanical weakening related to hydrocarbon production or water injection in oil and gas fields.

Hydrocarbon exploitation

Comparison of the results from mechanical tests performed on outcrop chalk samples indicates that EDL-related forces are a possible mechanism for the observed water weakening of chalk. The method that we developed to directly observe the electrostatic disjoining pressure could aid the tuning of injection brines designed to

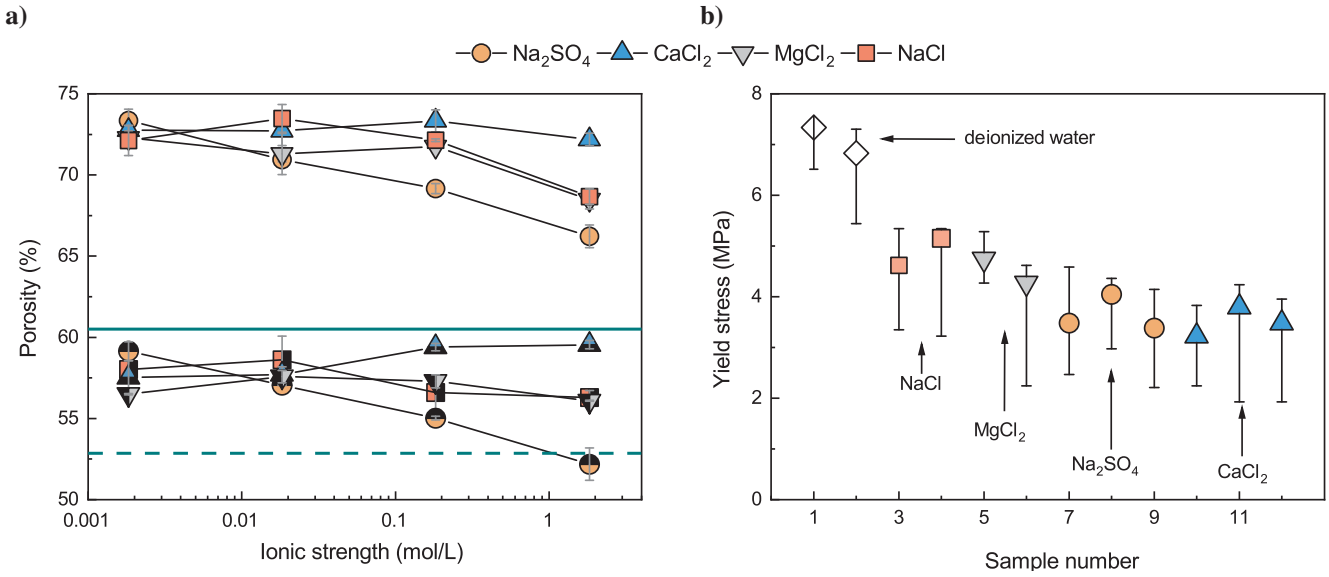

Figure 10. (a) Porosity of calcite powder column at the initial state and the final state. The reference lines (green solid, and green dashed) represent the average between two porosity measurements of samples saturated with ethylene glycol prior to and after centrifuging, respectively. (b) Peak strength of the Stevns chalk samples saturated with $CaCl_2$, $MgCl_2$, Na_2SO_4, NaCl, and deionized water. All samples failed due to pore collapse. Samples were loaded at near-oedometer conditions (horizontal strain approximately zero), with $\sigma_r \approx 0.3\sigma_a$. Symbols denote pore collapse, defined by Katika et al. (2015) as the point at which the linear fit to the elastic deformation region and the linear fit for the inelastic deformation region cross. The error bars denote the maximum and minimum values of the pore collapse stress taken as the initial deviation from elastic behavior (minimum) and the first point of purely inelastic behavior (maximum). (Figure 10b adapted from Katika et al., 2015).

minimize the disjoining pressure (aiming at the avoidance of pore collapse), for example, if it may induce subsidence that could damage surface installations, or to maximize the disjoining pressure (possibly promoting pore collapse) to increase recovery by compaction drive. This would be achieved by changing the fluid composition and ionic strength of saturating fluids in batch experiments and observing the resulting porosity in a settled column. These parameters could also be the key to control clay mobilization in the reservoir. Clay mobilization may be detrimental to pressure maintenance and hydrocarbon sweep during water injection, but it can also be used as a tertiary recovery method, possibly aiding physical plugging of previously swept parts of the porous network (Li, 2011).

CONCLUSION

In the course of this study, we devised a simple methodology to assess the effect of EDL-related forces in mineral powders saturated with brines prepared with mono- and divalent ions. For calcite and quartz, the EDL-related forces created a disjoining pressure between the grains that governed the settling porosity of the sediment column, whereas, for kaolinite, they also affected the flocculation behavior of the mixture. For all three test series, the observed behavior of the sediment can be related to the zeta potential data available in the literature.

Porosity data obtained from samples saturated with ethylene glycol allow us to establish a reference for the settling porosity in the absence of EDL-related forces. For quartz and calcite, the ethylene data showed a lower bound corresponding to brine-saturated samples with no net charge. However, for kaolinite samples, the structural charge distribution present in the kaolinite itself gives a higher porosity for ethylene glycol than for a brine at the point of zero net charge.

The weakening of chalk plugs observed in the literature as indicated by yield strength can be correlated to the EDL-related disjoining pressure for all tested brines. The apparent contradiction between sedimentation tests results conducted in this study and mechanical testing results from Katika et al. (2015) originated from different partial pressures of carbon dioxide between the two experiments.

The approach used in this study can be used to assess the magnitude of EDL-related forces of saturated sediments. It would be possible to use these techniques to evaluate the EDL-related forces using drill cuttings from a reservoir where water flooding is considered as a secondary or tertiary recovery method. These data could help to plan an optimal composition for the waterflooding fluid, depending on whether more or less compaction is required.

ACKNOWLEDGMENTS

We would like to thank Aksel Hiorth for feedback on the original manuscript and Merete Vadla Madland for constructive criticism of the conclusions. We thank the anonymous reviewers for their comments and suggestions. We acknowledge the previous studies performed in DTU on NMR characterization of saturated powders by Mohammad Monzurul Alam and Esther Rosenbrand. The research leading to these results has received funding from the Danish Hydrocarbon Research and Technology Centre under the Advanced Water Flooding program.

DATA AND MATERIALS AVAILABILITY

Data associated with this research are available and can be obtained by contacting the corresponding author.

REFERENCES

Al Mahrouqi, D., J. Vinogradov, and M. D. Jackson, 2017, Zeta potential of artificial and natural calcite in aqueous solution: Advances in Colloid and Interface Science, **240**, 60–76, doi: 10.1016/j.cis.2016.12.006.

Bergsaker, A. S., A. Røyne, A. Ougier-Simonin, J. Aubry, and F. Renard, 2016, The effect of fluid composition, salinity, and acidity on subcritical crack growth in calcite crystals: Journal of Geophysical Research: Solid Earth, **121**, 1631–1651.

Bovet, N., M. Yang, M. S. Javadi, and S. L. S. Stipp, 2015, Interaction of alcohols with the calcite surface: Physical Chemistry Chemical Physics, **17**, 3490–3496, doi: 10.1039/C4CP05235H.

Brunauer, S., P. H. Emmett, and E. Teller, 1938, Adsorption of gases in multimolecular layers: Journal of the American Chemical Society, **60**, 309–319, doi: 10.1021/ja01269a023.

Carles, P., and P. Lapointe, 2004, Water-weakening of under stress carbonates. New insights on pore volume compressibility measurements: Proceedings of the International Symposium of the Society of Core Analysts, 1–12.

Christensen, H. F., K. Hedegaard, and C. Høier, 2003, Shear failure induced by waterflooding of a fractured chalk?: Proceedings of the Second International Symposium on Rock Stress, 491–498.

Ciantia, M. O., R. Castellanza, and C. di Prisco, 2014, Experimental study on the water-induced weakening of calcarenites: Rock Mechanics and Rock Engineering, **48**, 441–461, doi: 10.1007/s00603-014-0603-z.

Clausen, L., and I. Fabricius, 2000, BET measurements: Outgassing of minerals: Journal of Colloid and Interface Science, **227**, 7–15, doi: 10.1006/jcis.2000.6880.

Coates, G. R., L. Xiao, and M. G. Prammer, 2000, NMR logging: Principles and applications: Halliburton Energy Services Publication.

Cook, C. C., and S. Jewell, 1996, Reservoir simulation in a North Sea reservoir experiencing significant compaction drive: SPE Reservoir Engineering, **11**, 48–53, doi: 10.2118/29132-PA.

Cooke, D. J., R. J. Gray, K. K. Sand, S. L. S. Stipp, and J. A. Elliott, 2010, Interaction of ethanol and water with the {10$\bar{1}$4} surface of calcite: Langmuir, **26**, 14520–14529, doi: 10.1021/la100670k.

De Gennaro, V., P. Delage, G. Priol, F. Collin, and Y. l. Cui, 2004, On the collapse behaviour of oil reservoir chalk: Géotechnique, **54**, 415–420, doi: 10.1680/geot.2004.54.6.415.

Derjaguin, B., and L. Landau, 1941, Theory of the stability of strongly charged lyophobic sols and of the adhesion of strongly charged particles in solutions of electrolytes: Acta Physicochemica U.R.S.S., **14**, 633–662.

Desarnaud, J., D. Bonn, and N. Shahidzadeh, 2016, The pressure induced by salt crystallization in confinement: Scientific Reports, **6**, 1–8, doi: 10.1038/srep30856.

Dunn, K. J., D. J. Bergman, and G. A. Latorraca, 2002, Nuclear magnetic resonance: Petrophysical and logging applications: Pergamon.

Ferris, A. P., and W. B. Jepson, 1975, The exchange capacities of kaolinite and the preparation of homoionic clays: Journal of Colloid and Interface Science, **51**, 245–259.

Fogden, A., M. Kumar, N. R. Morrow, and J. S. Buckley, 2011, Mobilization of fine particles during flooding of sandstones and possible relations to enhanced oil recovery: Energy & Fuels, **25**, 1605–1616, doi: 10.1021/ef101572n.

Gram, T. B., and I. L. Fabricius, 2015, Water weakening effects: Elasticity of reservoir chalk with partial fluid saturation: 3rd International Workshop on Rock Physics, 1–4.

Gupta, V., and J. D. Miller, 2010, Surface force measurements at the basal planes of ordered kaolinite particles: Journal of Colloid and Interface Science, **344**, 362–371, doi: 10.1016/j.jcis.2010.01.012.

Gutierrez, M., L. E. Øino, and K. Høeg, 2000, The effect of fluid content on the mechanical behaviour of fractures in chalk: Rock Mechanics and Rock Engineering, **33**, 93–117, doi: 10.1007/s006030050037.

Hellmann, R., P. Gaviglio, P. J. N. Renders, J.-P. Gratier, S. Békri, and P. Adler, 2002b, Experimental pressure solution compaction of chalk in aqueous solutions — Part 2: Deformation examined by SEM, porosimetry, synthetic permeability, and X-ray computerized tomography: The Geochemical Society, Special Publication: Water-Rock Interactions, Ore Deposits, and Environmental Geochemistry: A Tribute to David A. Crerar, 153–178.

Hellmann, R., P. J. N. Renders, J.-P. Gratier, and R. Guiguet, 2002a, Experimental pressure solution compaction of chalk in aqueous solutions — Part 1: Deformation behavior and chemistry: The Geochemical Society, Special Publication: Water-Rock Interactions, Ore Deposits, and Environmental Geochemistry: A Tribute to David A. Crerar, 129–152.

Hermansen, H., G. H. Landa, J. E. Sylte, and L. K. Thomas, 2000, Experiences after 10 years of waterflooding the Ekofisk Field, Norway: Journal of Petroleum Science and Engineering, **26**, 11–18, doi: 10.1016/S0920-4105(00)00016-4.

Hjuler, M. L., and I. L. Fabricius, 2009, Engineering properties of chalk related to diagenetic variations of Upper Cretaceous onshore and offshore chalk in the North Sea area: Journal of Petroleum Science and Engineering, **68**, 151–170, doi: 10.1016/j.petrol.2009.06.005.

Homand, S., and J. F. Shao, 2000, Mechanical behaviour of a porous chalk and water/chalk interaction — Part 1: Experimental study: Oil and Gas Science and Technology, **55**, 599–609, doi: 10.2516/ogst:2000045.

Huertas, F. J., L. Chou, and R. Wollast, 1999, Mechanism of kaolinite dissolution at room temperature and pressure — Part 2: Kinetic study: Geochimica et Cosmochimica Acta, **63**, 3261–3275, doi: 10.1016/S0016-7037(99)00249-5.

Israelachvili, J. N., 2011, Intermolecular and surface forces, Revised 3rd ed.: Academic Press.

Katika, K., M. Addassi, M. M. Alam, and I. L. Fabricius, 2015, The effect of divalent ions on the elasticity and pore collapse of chalk evaluated from compressional wave velocity and low-field nuclear magnetic resonance (NMR): Journal of Petroleum Science and Engineering, **136**, 88–99, doi: 10.1016/j.petrol.2015.10.036.

Keating, K., and R. Knight, 2007, A laboratory study to determine the effect of iron oxides on proton NMR measurements: Geophysics, **72**, E27–E32, doi: 10.1190/1.2399445.

Korsnes, R. I., M. V. Madland, and T. Austad, 2006, Impact of brine composition on the mechanical strength of chalk at high temperature: Eurock: Proceedings of the International Symposium of the International Society for Rock Mechanics, 133–140.

Li, Y., 2011, Oil recovery by low salinity water injection into a reservoir: A new study of tertiary oil recovery mechanism: Transport in Porous Media, **90**, 333–362, doi: 10.1007/s11242-011-9788-8.

Liu, J., L. Sandaklie-Nikolova, X. Wang, and J. D. Miller, 2013, Surface force measurements at kaolinite edge surfaces using atomic force microscopy: Journal of Colloid and Interface Science, **420**, 35–40, doi: 10.1016/j.jcis.2013.12.053.

Lord, C. J., C. L. Johlman, and D. W. Rhett, 1998, Is capillary suction a viable cohesive mechanism in chalk?: Proceedings of the SPE/ISRM Eurock, **98**, 479–485.

Lu, Y., N. F. Najafabadi, and A. Firoozabadi, 2017, Effect of temperature on wettability of oil/brine/rock systems: Energy & Fuels, **31**, 4989–4995, doi: 10.1021/acs.energyfuels.7b00370.

Ma, C., and R. A. Eggleton, 1999, Cation exchange capacity of kaolinite: Clays and Clay Minerals, **47**, 174–180, doi: 10.1346/CCMN.

Madland, M. V., A. Hiorth, E. Omdal, M. Megawati, T. Hildebrand-Habel, R. I. Korsnes, S. Evje, and L. M. Cathles, 2011, Chemical alterations induced by rock-fluid interactions when injecting brines in high porosity chalks: Transport in Porous Media, **87**, 679–702, doi: 10.1007/s11242-010-9708-3.

Madsen, L., 2001, Surface charge of calcite, *in* P. Somasundaran, ed., Encyclopedia of surface and colloid science: CRC Press, 4982–4994.

Megawati, M., A. Hiorth, and M. V. Madland, 2013, The impact of surface charge on the mechanical behavior of high-porosity chalk: Rock Mechanics and Rock Engineering, **46**, 1073–1090, doi: 10.1007/s00603-012-0317-z.

Meiboom, S., and D. Gill, 1958, Modified Spiniecho method for measuring nuclear relaxation times: Review of Scientific Instruments, **29**, 688–691, doi: 10.1063/1.1716296.

Nermoen, A., R. I. Korsnes, A. Hiorth, and M. V. Madland, 2015, Porosity and permeability development in compacting chalks during flooding of nonequilibrium brines: Insights from long-term experiment: Journal of Geophysical Research: Solid Earth, **120**, 2935–2960 .

Nermoen, A., R. I. Korsnes, E. V. Storm, T. Stødle, M. V. Madland, and I. L. Fabricius, 2018, Incorporating electrostatic effects into the effective stress relation — Insights from chalk experiments: Geophysics, **83**, no. 3, MR123–MR135, doi: 10.1190/geo2016-0607.1.

Newman, G., 1983, The effect of water chemistry on the laboratory compression and permeability characteristic of North Sea chalks. Journal of Petroleum Technology, **35**, 976–980, doi: 10.2118/10203-PA.

Nyström, R., M. Lindén, and J. B. Rosenholm, 2001, The influence of Na^{+}, Ca^{2+}, Ba^{2+}, and La^{3+} on the ζ potential and the yield stress of calcite dispersions: Journal of Colloid and Interface Science, **242**, 259–263, doi: 10.1006/jcis.2001.7766.

O'Brien, N. R., 1971, Fabric of kaolinite and illite floccules: Clays and Clay Minerals, **19**, 353–359, doi: 10.1346/CCMN.

Ovens, J. E. V., F. P. Larsen, and D. R. Cowie, 1998, Making sense of water injection fractures in the Dan field: SPE Reservoir Evaluation & Engineering, **1**, 556–566, doi: 10.2118/52669-PA.

Pierre, A., J. M. Lamarche, R. Mercier, A. Foissy, and J. Persello, 1990, Calcium as potential determining ion in aqueous calcite suspensions: Journal of Dispersion Science and Technology, **11**, 611–635, doi: 10.1080/01932699008943286.

Pourchet, S., I. Pochard, F. Brunel, and D. Perrey, 2013, Chemistry of the calcite/water interface: Influence of sulfate ions and consequences in terms of cohesion forces: Cement and Concrete Research, **52**, 22–30, doi: 10.1016/j.cemconres.2013.04.002.

Quan, X., W. Jiazhong, Q. Jishun, L. Qingjie, M. Desheng, L. Li, and L. Manli, 2012, Investigation of electrical surface charges and wettability alteration by ions matching waterflooding: International Symposium of the Society of Core Analysts, 1–12.

Risnes, R., H. Haghighi, R. I. Korsnes, and O. Natvik, 2003, Chalk-fluid interactions with glycol and brines: Tectonophysics, **370**, 213–226, doi: 10.1016/S0040-1951(03)00187-2.

Risnes, R., M. V. Madland, M. Hole, and N. K. Kwabiah, 2005, Water weakening of chalk — Mechanical effects of water-glycol mixtures: Journal of Petroleum Science and Engineering, **48**, 21–36, doi: 10.1016/j.petrol.2005.04.004.

Røgen, B., and I. L. Fabricius, 2002, Influence of clay and silica on permeability and capillary entry pressure of chalk reservoirs in the North Sea: Petroleum Geoscience, **8**, 287–293, doi: 10.1144/petgeo.8.3.287.

Røyne, A., K. N. Dalby, and T. Hassenkam, 2015, Repulsive hydration forces between calcite surfaces and their effect on the brittle strength of calcite-bearing rocks: Geophysical Research Letters, **42**, 4786–4794, doi: 10.1002/2015GL064365.

Schroeder, C., A.-P. Bois, V. Maury, and G. Halle, 1998, Results of tests performed in laboratory on Lixhe chalk to calibrate water/ chalk models. Water/chalk (or collapsible soil) interaction — Part 2: EurockT98: SPE/ISRM Programme Committee, 505–514.

Sohal, M. A., G. Thyne, and E. G. Søgaard, 2016, Review of recovery mechanisms of ionically modified waterflood in carbonate reservoirs: Energy & Fuels, **30**, 1904–1914, doi: 10.1021/acs.energyfuels.5b02749.

Song, J., Y. Zeng, L. Wang, X. Duan, M. Puerto, W. G. Chapman, S. L. Biswal, and G. J. Hirasaki, 2017, Surface complexation modeling of calcite zeta potential measurements for characterizing carbonate wettability: Journal of Colloid and Interface Science, **506**, 169–179, doi: 10.1016/j.jcis.2017.06.096.

Stipp, S. L. S., 1999, Toward a conceptual model of the calcite surface: Hydration, hydrolysis, and surface potential: Geochimica et Cosmochimica Acta, **63**, 3121–3131, doi: 10.1016/S0016-7037(99)00239-2.

Tansel, B., J. Sager, T. Rector, J. Garland, R. F. Strayer, L. Levine, M. Roberts, M. Hummerick, and J. Bauer, 2006, Significance of hydrated radius and hydration shells on ionic permeability during nanofiltration in dead end and cross flow modes: Separation and Purification Technology, **51**, 40–47.

Van Olphen, H., 1963, An introduction to clay colloid chemistry: For clay technologists, geologists, and soil scientists: Interscience Publishers.

Verwey, E. J. W., and J. Th. H. Overbeek, 1948, Theory of the stability of lyophobic colloids: The Journal of Physical and Colloid Chemistry, **51**, 631–636, doi: 10.1021/j150453a001.

Weast, R. C., 1989, CRC handbook of chemistry and physics: CRC Press.

Woessner, D. E., 1980, An NMR investigation into the range of the surface effect on the rotation of water molecules: Journal of Magnetic Resonance (1969), **39**, 297–308, doi: 10.1016/0022-2364(80)90138-9.

Yukselen, Y., and A. Kaya, 2003, Zeta potential of kaolinite in the presence of alkali, alkaline earth and hydrolyzable metal ions: Water, Air, and Soil Pollution, **145**, 155–168, doi: 10.1023/A:1023684213383.